Robotica (2014) volume 32, pp. 889–905. © Cambridge University Press 2013
doi:10.1017/S0263574713001100

A non-overconstrained variant of the Agile Eye with a special decoupled kinematics

Chin-Hsing Kuo†,*, Jian S. Dai‡ and Giovanni Legnani§

†*Department of Mechanical Engineering, National Taiwan University of Science and Technology, Taipei 106, Taiwan*
‡*Centre for Robotics Research, King's College London, University of London, London WC2R 2LS, UK*
§*Dip. Ingegneria Meccanica e Industriale, Università di Brescia, 25123 Brescia, Italy*

(Accepted October 29, 2013. First published online: December 5, 2013)

SUMMARY
A non-overconstrained three-DOF parallel orientation mechanism that is kinematically equivalent to the Agile Eye is presented in this paper. The output link (end-effector) of the mechanism is connected to the base by one spherical joint and by another three identical legs. Each leg comprises of, in turns from base, a revolute joint, a universal joint, and three prismatic joints. The three lower revolute joints are active joints, while all other joints are passive ones. Based on a special configuration, some three projective angles of the end-effector coordinates are fully decoupled with respect to the input actuated joints, that is, by actuating any revolute joint the end-effector rotates in such a way that the corresponding projective angle changes with the same angular displacement. The fully decoupled motion is analyzed geometrically and proved theoretically. Besides, the inverse and direct kinematics solutions of the mechanism are provided based on the geometric reasoning and theoretical proof.

KEYWORDS: Decoupled motion; Parallel wrist mechanism; Spherical parallel manipulator; Spherical mechanism.

1. Introduction

Parallel orientation mechanism, also known as the spherical parallel manipulator or parallel wrist mechanism, is a mechanism that, based on in-parallel actuations, generates purely rotational motion with respect to the fixed coordinate over its output link. From the numerous inventions, the *Agile Eye*[1–3] robot is one of the most well-known parallel orientation mechanisms for its compact structure and excellent rotational ability. The mechanism structure of Agile Eye is quite simple indeed. It is composed by the base, the end-effector, and three legs, each having three revolute joints, which leads to an overconstrained mechanism structure. Therefore, in order to make the mechanism mobile, all the axes of the nine revolute joints must converge at a fixed point where the center of rotation is. Under such a requirement, the mechanism will demand a high-standard manufacturing and assembling precisions for making it workable.

While an overconstrained mechanism requires high-standard manufacturing and assembling precision, a non-overconstrained counterpart has naturally found its excellence in compensating such problems. Compared to the overconstrained mechanism, a non-overconstrained mechanism normally requests fewer alignment requirements, which makes it more accessible in practical applications.

Kinematically non-redundant parallel orientation mechanisms are one type of non-overconstrained mechanisms. Generally, a kinematically non-redundant parallel orientation mechanism can be constructed in two different ways. First, an n-degree-of-freedom (DOF) parallel orientation mechanism is made up of the base, the output link (i.e., the end-effector), and n serial chains (or so-called the "legs" in parallel manipulators) that collaboratively connect the end-effector to the base. Subject to the structural constraints provided by the n serial chains, the output link is

* Corresponding author. E-mail: chkuo717@mail.ntust.edu.tw

prohibited from moving in any direction so it can only rotate about a fixed point in space. Normally, one joint in each chain is selected to be actuated so that the n-DOF pure rotation can be controlled by the n joints together. Based on this concept, many parallel orientation mechanisms have been proposed and extensively studied. For example, Kong and Gosselin[4,5] proposed the type synthesis of 3-DOF spherical parallel manipulators by using screw theory. Fang and Tsai[6] also addressed a screw-theoretic-based method for the type synthesis of the 3-DOF spherical parallel manipulator with same legs. Karouia and Hervé[7] synthesized a group of 3-DOF spherical parallel mechanisms having asymmetric structures. Hess-Coelho[8] summarized a list of possible structures for parallel wrists and suggested a qualitative procedure for evaluating the wrist mechanisms. Many other parallel orientation mechanisms using this concept have been exhaustively studied.[1,9–18] Furthermore, some special parallel orientation mechanisms have been built by using parallelograms as the serial chains.[19,20] In general, an n legs, n-DOF parallel orientation mechanism requires the inclusion of revolute joints whose axes intersect at a common point for making up with the spherical motion.

Oppositely, the second type requires no necessity of the revolute joints and their intersecting axes. Instead, it includes one additional joint into the motion that could completely constrain the motion of the output link. The added joint, normally a universal or spherical joint, articulates the output link to the base such that the available motion space of the output link is completely defined by the joint. The n serial chains, each containing one actuated joint, are then structured in a way that each chain will not contribute additional motion constraints to the output link. The most well-known parallel orientation mechanism for this type is probably the 3-DOF 3SPS/S (three spherical-prismatic-spherical-joint legs and one additional spherical joint connecting the end-effector and the base) parallel manipulator. Some literatures have studied this mechanism exhaustively.[21–24] Some other 3-DOF parallel orientation mechanisms using a constrained joint can be found in Hess-Coelho.[8] In addition, there have been few parallel orientation mechanisms with two DOFs synthesized by using this concept.[25,26] Some special non-redundant parallel mechanisms with decoupled rotational and translational motion were also put forward based on using this concept (e.g., see Kuo and Dai[27]).

A kinematically non-redundant parallel orientation mechanism with a special decoupled kinematics is analyzed in this paper. The proposed parallel manipulator is a variant of the Agile Eye robot but with non-overconstrained structure. It consists of three active legs and one passive spherical joint that connects the end-effector to the base. In each leg, a revolute joint mounted on the base is selected for actuation. Under a specific joint configuration, the three rotational DOFs, that are described by the projective angles of moving coordinate system on the fixed coordinate system, of the end-effector are fully decoupled. In the following, the concepts of projective angles and decoupled motion are reviewed first. Then, the structure and geometric arrangement of this mechanism are introduced. The relationship between the projective angles and the rotation matrix is discussed. The inverse and direct kinematics solutions of the mechanism are studied. And, the geometric reasoning and algebraic verification of the inverse and direct kinematics solutions are discussed.

2. Preliminary

2.1. Projective angles

The concept of projective displacement representation[27,28] is adopted in this paper. Let $O(x, y, z)$ and $E(u, v, w)$ be the referencing coordinate systems fixed in space and attached on end-effector, respectively. Accordingly, we can describe the location of end-effector by using the position vector of the origin of coordinate system E and using *some* projective angles of coordinate system E to define the angular displacements of the end-effector. Since each coordinate axis of E can be projected onto several different planes in O, the location of the end-effector may have many different representations when different projective angles are employed. We will indicate by the symbol ${}^{u}\theta_{ab}$ the projective angle of vector $\mathbf{u}$ in the plane ab, which is the orientation of the projection of $\mathbf{u}$ in the plane ab, i.e., ${}^{u}\theta_{ab} = \text{atan2}\,(u_b, u_a)$ where atan2(c, d) is the four quadrants extension of atan(c/d). For example, Fig. 1 gives two projective displacement representations for the end-effector. In Fig. 1(a), the coordinate transformation between $O(x, y, z)$ and $E(u, v, w)$ is described by a position vector and an angular displacement vector. The position vector, $\mathbf{e}$, is measured from the origin of coordinate system O to the origin of coordinate system E, while the angular displacement vector, $[{}^{w}\theta_{xz}, {}^{w}\theta_{yz}, \theta_w]^{\mathrm{T}}$, is made of two projective angles and one spin angle, all defined by the w-axis of coordinate system E.

https://doi.org/10.1017/S0263574713001100 Published online by Cambridge University Press

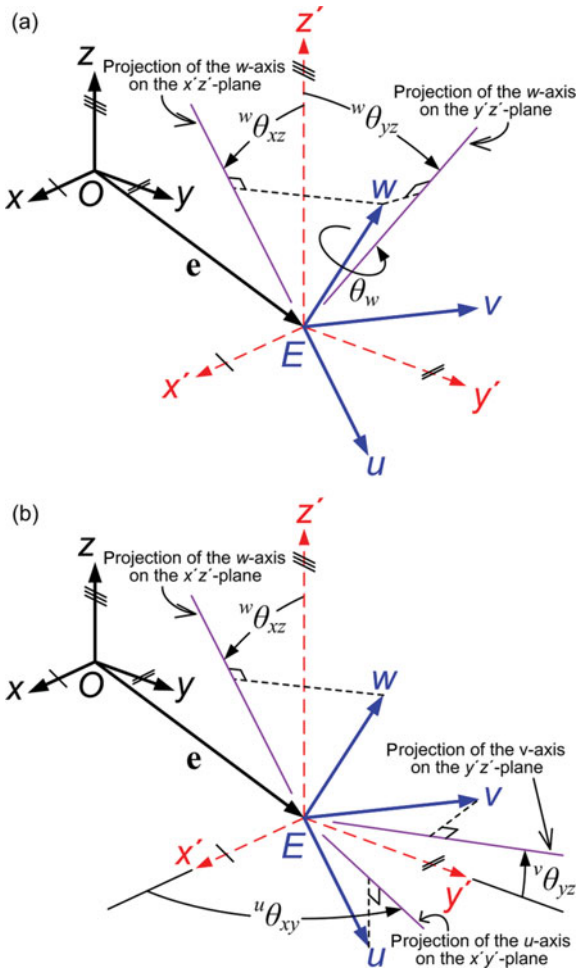

Fig. 1. (Colour online) Projective-angle representation: (a) Angular displacement expressed by one axis of E; (b) Angular displacement expressed by three axes of E.

The two projective angles, $^{w}\theta_{xz}$ and $^{w}\theta_{yz}$, are measured equivalently from the z-axis to the projections of the w-axis on the xz- and yz-planes, respectively. The spin angle, θ_w, is specified to define the spin rotation of the coordinate system E about the w-axis. Alternatively, we may also formulate the angular displacements of the moving coordinate system E through the three coordinate axes of E, rather than through the w-axis only. For example, Fig. 1(b) uses three projective angles, $^{u}\theta_{xy}$, $^{v}\theta_{yz}$, and $^{w}\theta_{xz}$, which are respectively governed by axes u, v, and w, to define the angular displacements of $E(u, v, w)$ with respect to $O(x, y, z)$.

2.2. Decoupled parallel manipulators

Decoupled parallel manipulators refer to the parallel manipulator whose some or all the output motion variables are independently controllable by actuators. The advantages of decoupled parallel manipulators are diversified, e.g., decoupled kinematic characteristics, variable actuation strategy for different tasks, simplified kinematic analysis, easier motion planning and control scheme, etc. For investigating the decouplebility, Jin *et al.*[29] classified the decoupled motion of a 6-DOF parallel manipulator into *complete coupling*, *group decoupling*, and *complete decoupling*. Another classification was reported in Legnani *et al.*[30] in which the decoupling with respect to direct/inverse kinematic as well as with respect to local kinetostatic behavior described by the Jacobian matrix were discussed.

In this paper, we suggest another classification for general decoupled parallel manipulators with mobility two to six. For a non-redundant f-DOF parallel manipulator, let $e_1, e_2, \ldots, e_f$ be the f independent output motion variables (e.g., displacement, velocity, or acceleration vectors) of the

https://doi.org/10.1017/S0263574713001100 Published online by Cambridge University Press

end-effector and $a_1, a_2, \ldots, a_f$ be the f independent actuators. The degree of (de)coupling can be classified as follows:

Completely coupled. In this type, each independent actuator has contribution to every output motion variable of the end-effector. Mathematically, this kind of relationship can be expressed as

$$e_1, e_2, \ldots, e_f = f(a_1, a_2, \ldots, a_f), \quad \text{for } 1 < f \leq 6. \tag{1}$$

Partially decoupled. In this type, some motion variables of the end-effector are independent of some actuators, i.e.,

$$\begin{cases} e_1 = f_1(a_1) \\ e_2 = f_2(a_2) \\ \vdots \\ e_i = f_i(a_i) \\ e_{i+1}, e_{i+2}, \ldots, e_f = f_{i+1}(a_1, a_2, \ldots, a_f) \end{cases}, \quad \text{for} \begin{cases} 1 \leq i < f \leq 6 \\ A_i = \left\{ a_{k_1}, a_{k_2}, \ldots, a_{k_m} \,|\, 1 \leq k_m < f \right\} \end{cases}. \tag{2}$$

Fully decoupled. In this type, each motion variable of the end-effector is controlled by one corresponding actuator independently, i.e.,

$$\begin{cases} e_1 = f_1(a_1) \\ e_2 = f_2(a_2) \\ \vdots \\ e_f = f_f(a_f) \end{cases}, \quad \text{for } 1 < f \leq 6. \tag{3}$$

Notice that, without losing generality, the output motion variables of end-effector, e_f, and the input motion variables, a_f, can be either a (projective) displacement, velocity, or acceleration vector. In other words, for a fully decoupled manipulator, each actuator may be in charge of controlling one independent displacement, velocity, or acceleration vector element of the end-effector. In what follows, we will present a parallel manipulator that has fully decoupled projective angles, that is, each actuator can independently control a projective angle of the end-effector's coordinate.

3. Description of the Mechanism

The proposed parallel wrist mechanism is shown in Fig. 2. The end-effector is connected to the base by one spherical joint (S-joint) and by another three in-parallel legs, respectively. The three legs possess the same topological structure, which is composed of, as read from base to the end-effector, a revolute joint (R-joint), a universal joint (U-joint), and three consecutive prismatic joints (P-joints). According to the Grübler-Kutzbach criterion, the mobility of the mechanism, f, can be calculated as:

$$f = \lambda(n - j - 1) + \sum f_i = 3, \tag{4}$$

where $\lambda = 6$ is the degrees of freedom of the space, $n = 14$ is the number of links, $j = 16$ is the number of joints, and $\sum f_i = 21$ is the total degrees of freedom of the joints. As a result, the mobility of the mechanism is three, and this mechanism is non-overconstrained. Besides, it can be quickly realized that the mechanism can output a 3-DOF spherical motion at the end-effector that can rotate about the center of the S-joint only. The mobility analysis of Eq. (4) can be verified by an analysis of the Jacobian of the mechanisms (see appendix B.2 of Legnani *et al.*[30]).

For analyzing the kinematics of the mechanism, two Cartesian coordinate systems $A(x, y, z)$ and $B(u, v, w)$ are attached to the base and end-effector, respectively. As shown in Fig. 2, in order to

https://doi.org/10.1017/S0263574713001100 Published online by Cambridge University Press

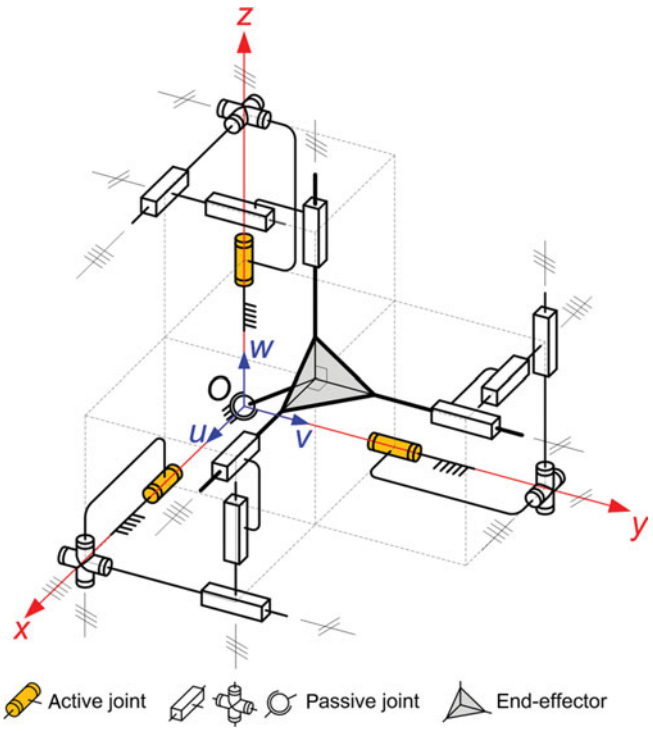

Fig. 2. (Colour online) A 3-DOF parallel orientation mechanism with fully decoupled projective angles.

simplify the analysis, we assume that the origin of the fixed coordinate A is located at the center of the S-joint, O, and the origin of the moving coordinate B is initially coincident with O. Since the end-effector can only rotate about the center of the S-joint, the origin of the moving coordinate will be always pivoted at O. Furthermore, we assume that the moving coordinate is coincident with the fixed coordinate at the initial position, i.e., the u-, v-, and w-axis are initially pointing at the x-, y-, and z-direction, respectively.

For achieving the fully decoupled condition, the mechanism is initially configured in a way that meets the following geometric and actuation conditions:

(1) The axes of the three R-joints are coincident with the x-, y-, and z-axis, respectively.
(2) In each leg, the axis of the R-joint passes through the center of the U-joint.
(3) In each leg, the two axes of the U-joint are perpendicular to the axis of the R-joint of this leg.
(4) In each leg, the three P-joints can be arbitrarily deposed provided that all the joint directions are not coplanar.
(5) In each leg, the R-joint is selected as the actuated joint, whereas all the others are passive.

The above geometric arrangements are as shown in Fig. 2. Note that conditions (1) and (2) remain during the full cycle of motion but condition (3) may be destroyed after the mechanism has an infinitesimal displacement.

In accordance with the above geometric conditions, we further assemble the mechanism at a special initial configuration for simplifying the analysis. Without violating condition (3), we align the two axes of the U-joint in each leg with the two axial directions other than the R-joint's. For example, if the R-joint is directed at the x-axis, the two axes of the U-joint in this leg are initially aligned with the y- and z-direction, respectively. Also, without violating condition (4), we place the three P-joints in each leg pointing at the three axial directions of the fixed frame, respectively. Since the kinematics of a prismatic joint is independent of the joint position, the articulation order of the three allocated joint orientation can be freely altered. Accordingly, a feasible joint configuration is defined as illustrated by the structural graph in Fig. 3. In this graph, the characters adjacent to the line segments represent the type of the joints whereas the subscripts of the characters denote the orientation(s) of the joint at the initial mechanism configuration. The corresponding mechanism is shown in Fig. 2.

https://doi.org/10.1017/S0263574713001100 Published online by Cambridge University Press

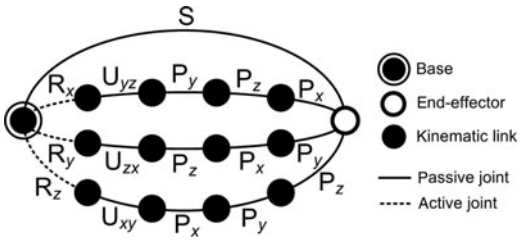

Fig. 3. Structural graph of the mechanism in Fig. 2.

It is interesting to note that, since the prismatic joints do not alter the orientation of the platform, the proposed manipulator is kinematically equivalent to the *Agile Eye*.[1–3] However, while Agile Eye is an overconstrained spherical mechanism, the presented design is a non-overconstrained spatial mechanism.

4. Decoupled Motion Analysis

Now we prepare to examine the fully decoupled kinematics of this mechanism. We will show that the mechanism is with fully decoupled projective angles, that is, by actuating any of the lower R-joints it makes the end-effector rotating in such a way that the corresponding projective angle changes by the same quantity. Note that this does not mean that the angular velocity of the end-effector is equal to the time derivative of the input joints. In fact, due to the non-integrability of the angular velocity vector, such an integration does not produce a value that represents the angular position (e.g., see appendix A of Legnani *et al.*[30]). Here, the decoupled motion implies that the partial derivative of each projective angle (θ) with respect to the corresponding input joint (α) is equal to 1 and with respect to the other joints are zeros; in other words the Jacobian is unitary as

$$\frac{\partial\left({}^{v}\theta_{yz},\,{}^{w}\theta_{zx},\,{}^{u}\theta_{xy}\right)}{\partial\left(\alpha_x,\alpha_y,\alpha_z\right)}=\begin{bmatrix}1&0&0\\0&1&0\\0&0&1\end{bmatrix}.$$

Since the three legs have the same topology and are configured in a similar way, here we only analyze the leg mounted at the x-axis for illustration. The analysis of the other two legs can be done by following the same logic. First of all, Fig. 4 depicts the geometry of the leg mounted on the x-axis. In this figure, A_x indicates the point at which the U-joint locates. E is a point on the end-effector at which the three P-joints attached on the end-effector intersect. $\mathbf{a}_x$ is the position vector measured from point O to A_x, whereas vector $\mathbf{e}$ is the position vector measured from point O to E. $\mathbf{d}_{1,x}$, $\mathbf{d}_{2,x}$, and $\mathbf{d}_{3,x}$ are the position vectors representing the motion of the three consecutive P-joints in the leg, where $\mathbf{d}_{1,x}$ is measured from A_x to point R_x, $\mathbf{d}_{2,x}$ is measured from R_x to point B_x, and $\mathbf{d}_{3,x}$ is measured from E to B_x. $\mathbf{d}_{3,y}$ and $\mathbf{d}_{3,z}$ denote two P-joints of the other two legs that are attached to the end-effector and are both measured outward from E. $\mathbf{u}_{2,x}$ is the unit vector of first axis of the U-joint connected with the R-joint, whereas $\mathbf{u}_{3,x}$ is the unit vector of the second axis of the U-joint connected with the first P-joint (as read from base). Π_{Ax} is the plane parallel to yz-plane and containing point A_x. Lying on Π_{Ax}, $\mathbf{y}'$ and $\mathbf{z}'$ are two unit vectors passing through A_x and pointing at the y- and z-direction, respectively. α_x is the angle between $\mathbf{z}'$ and $\boldsymbol{u}_{2,x}$, which represents the angular displacement of the actuated joint.

Owing to the specific joint configuration, there are some geometric constraints pertinent to these position vectors. First, due to the geometric relationship between the R-joint and the U-joint, point A_x will be a fixed point in space and $\mathbf{u}_{2,x}$ will always lie on Π_{Ax}. Since the three consecutive P-joints are configured with an orthogonal pose, vector $\mathbf{d}_{1,x}$ will be always perpendicular to $\mathbf{d}_{2,x}$ and so is $\mathbf{d}_{2,x}$ to $\mathbf{d}_{3,x}$. Therefore, R_x and B_x will be the two perpendicular foots between the three vectors. Furthermore, thanks to the predefined moving coordinate and the orthogonal condition among all the P-joints in the mechanism, the following conditions will be satisfied at any

https://doi.org/10.1017/S0263574713001100 Published online by Cambridge University Press

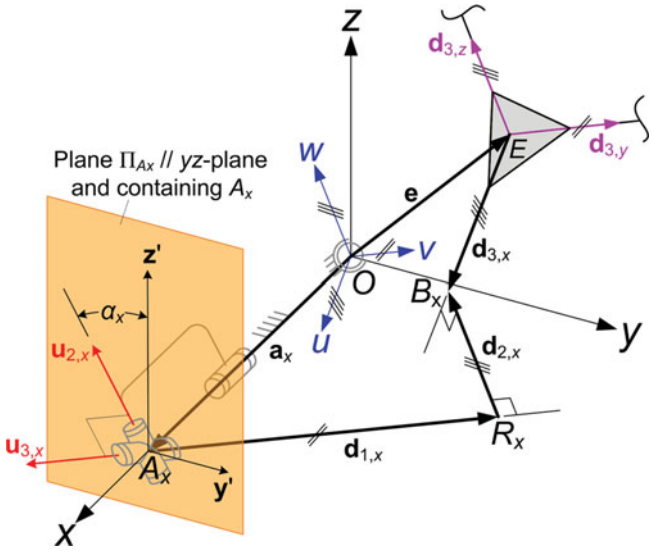

Fig. 4. (Colour online) The geometry of the leg mounted on the x-axis.

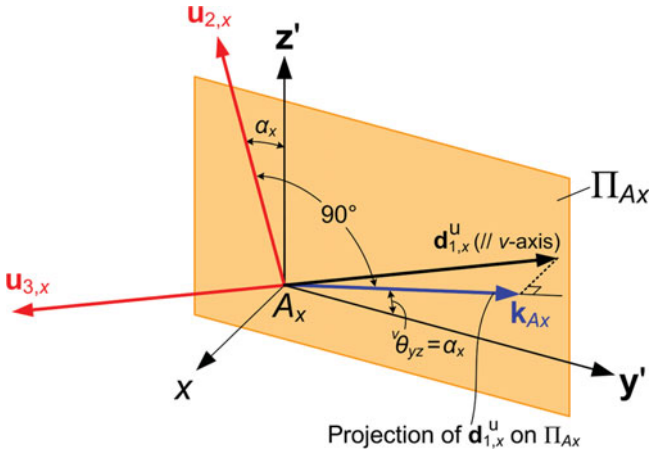

Fig. 5. (Colour online) Geometrical interpretation of the input angle.

instant:

$$\mathbf{u}//\mathbf{d}_{3,x}, \tag{5a}$$

$$\mathbf{v}//\mathbf{d}_{3,y}//\mathbf{d}_{1,x}, \tag{5b}$$

$$\mathbf{w}//\mathbf{d}_{3,z}//\mathbf{d}_{2,x}, \tag{5c}$$

where $\mathbf{u}$, $\mathbf{v}$, and $\mathbf{w}$ are the unit vectors along the u-, v-, and w-axis of the moving coordinate and symbol "//" indicates that the vectors at the two sides of the symbol are parallel. Particularly, it is noticed that in Eq. (5b) the axial direction of the first P-joint is parallel to the v-axis. We further inspect this geometric relationship by considering vector $\mathbf{u}_{2,x}$ on plane Π_{Ax}. Referring to Fig. 4, $\mathbf{d}^{u}_{1,x}$ is the unit vector of $\mathbf{d}_{1,x}$. Since $\mathbf{d}^{u}_{1,x}$ is always coincident with the second axis of the U-joint (i.e., $\mathbf{d}^{u}_{1,x} = -\mathbf{u}_{3,x}$ in Fig. 5), it will be always perpendicular to $\mathbf{u}_{2,x}$. Recall that $\mathbf{u}_{2,x}$ always lies on Π_{Ax}. Therefore, provided that $\mathbf{d}^{u}_{1,x}$ is not perpendicular to Π_{Ax}, the projective vector, $\mathbf{k}_{Ax}$, of $\mathbf{d}^{u}_{1,x}$ on Π_{Ax} will be always perpendicular to $\mathbf{u}_{2,x}$. Since $\mathbf{d}^{u}_{1,x}$ is parallel to the v-axis of the moving coordinate and Π_{Ax} is parallel to the yz-plane of the fixed coordinate, it turns out that the projection of vector $\mathbf{v}$ on the yz-plane will be always perpendicular to the projection of $\boldsymbol{u}_{2,x}$ on the yz-plane. Furthermore, from Fig. 5, we can observe that the angle between $\mathbf{k}_{Ax}$ and $\mathbf{y}'$, ${}^{v}\theta_{yz}$, is identical to that between $\boldsymbol{u}_{2,x}$ and $\mathbf{z}'$, i.e., α_x.

https://doi.org/10.1017/S0263574713001100 Published online by Cambridge University Press

The above geometric condition shows an interesting input–output relationship between the actuated joint and the end-effector. First, it proves that the projection of the v-axis of the moving coordinate on the yz-plane will be always perpendicular to the unit vector of the first axis of the U-joint on the x-axis. In other words, the projective angular displacement of the v-axis on the yz-plane will be completely defined by the angular displacement of the R-joint at the x-axis. Furthermore, the amount of this projective displacement (${}^{v}\theta_{yz}$) will be equal to that of the angular displacement of the actuated joint (α_x). However, we should notice that the revolute joints of each leg form a Cardanic sequence and so the same angular position of the end-effector may be reached by two different sets of joint angles; in fact, the two sequences $Q_1 = \{\alpha, \beta, \gamma\}$ and $Q_2 = \{\alpha + \pi, -\beta, \gamma + \pi\}$ produce the same result. Therefore, by following the same deduction above, we can find the similar input–output relationships in the other two legs. Consequently, a fully decoupled kinematics in terms of the projective angles can be expressed as

$$\begin{bmatrix} {}^{v}\theta_{yz} \\ {}^{w}\theta_{zx} \\ {}^{u}\theta_{xy} \end{bmatrix} = \begin{bmatrix} 1 & 0 & 0 \\ 0 & 1 & 0 \\ 0 & 0 & 1 \end{bmatrix} \begin{bmatrix} \alpha_x \\ \alpha_y \\ \alpha_z \end{bmatrix} + \begin{bmatrix} k_x \\ k_y \\ k_z \end{bmatrix} \pi, \tag{6}$$

where (${}^{v}\theta_{yz}$, ${}^{w}\theta_{zx}$, ${}^{u}\theta_{xy}$) represents the projective displacements of the v-, w-, and u-axis on the yz-, zx-, and xy-plane, ($\alpha_x, \alpha_y, \alpha_z$) indicates the angular displacements of the actuated joint on the x-, y-, and z-axis, and k_x, k_y, and k_z, are either 0 or 1 implying the two assemblies of the leg. Equation (6) states that:

(a) the projective angles ${}^{v}\theta_{yz}$, ${}^{w}\theta_{zx}$, and ${}^{u}\theta_{xy}$ are fully decoupled; and
(b) the projective angles ${}^{v}\theta_{yz}$, ${}^{w}\theta_{zx}$, and ${}^{u}\theta_{xy}$ are independently determined by the input angles $\alpha_x, \alpha_y, \alpha_z$, respectively.

Note that such a projective-angle-based decoupled kinematics is also valid in the Agile Eye robot. The proof can be deducted by following the same logic above.

5. Relationship between the Projective Angles and Rotation Matrix

In this section, we will examine the relationship between the rotation matrix expressing the angular position of the end-effector relating to the corresponding projective angles. It will show that, while the rotation matrix is specified, there will be one unique possible configuration corresponding to the set of projective vectors. The fact will be further used for verifying the inverse and direct kinematic solutions of the manipulator in next sections.

Let us consider the rotation matrix, ${}^{A}\mathbf{R}_{B}$, which transforms the fixed coordinate A to the moving coordinate B by the direction cosines of the unit vectors **u**, **v**, and **w**; that is

$${}^{A}\mathbf{R}_{B} = [\mathbf{u}, \mathbf{v}, \mathbf{w}] = \begin{bmatrix} u_x & v_x & w_x \\ u_y & v_y & w_y \\ u_z & v_z & w_z \end{bmatrix}.$$

It is obvious that there exists a parallelism between the end-effector's coordinate axes u, v, and w and the axis of the second revolute joint of each leg, that is, $u//d_{1,z}$, $v//d_{1,x}$, $w//d_{1,y}$. Let vector **q** collect the joint displacement coordinates of the actuators and vector **s** represent the projective angles of the moving coordinate axes on the appropriate planes, i.e.,

$$\mathbf{q} = \begin{bmatrix} \alpha_x \\ \alpha_y \\ \alpha_z \end{bmatrix} \tag{7}$$

and

$$\mathbf{s} = \begin{bmatrix} {}^{v}\theta_{yz} \\ {}^{w}\theta_{zx} \\ {}^{u}\theta_{xy} \end{bmatrix} = \begin{bmatrix} \alpha'_x \\ \alpha'_y \\ \alpha'_z \end{bmatrix}, \tag{8}$$

https://doi.org/10.1017/S0263574713001100 Published online by Cambridge University Press

where symbols α' are synonymous with θ and are here used to emphasize the links between the projective angles θ and the input angles α. Note that we have shown in the previous section that there exists a decoupled relationship between vectors $\mathbf{q}$ and $\mathbf{s}$, i.e., $\alpha'_x = \alpha_x + k_x\pi$, $\alpha'_y = \alpha_y + k_y\pi$, and $\alpha'_z = \alpha_z + k_z\pi$, $k_x, k_y, k_z, = 0$ or 1.

To convert ${}^A\mathbf{R}_B$ to $\mathbf{s}$ we need to observe the projections of axis v on the yz-plane, of axis w on the xz-plane, and of axis u on the xy-plane. So, we obtain

$$\mathbf{s} = \begin{bmatrix} {}^v\theta_{yz} \\ {}^w\theta_{zx} \\ {}^u\theta_{xy} \end{bmatrix} = \begin{bmatrix} \alpha'_x \\ \alpha'_y \\ \alpha'_z \end{bmatrix} = \begin{bmatrix} \text{atan2}(v_z, v_y) \\ \text{atan2}(w_x, w_z) \\ \text{atan2}(u_y, u_x) \end{bmatrix}. \tag{9}$$

So, given the rotation matrix (i.e., the angular position of the end-effector), the projective angles are univocally determined.

Note that each leg is an Eulerian/Cardanic sequence. So, the directions of unit vectors $\mathbf{u}$, $\mathbf{v}$, and $\mathbf{w}$ can be expressed in the rotation matrix in function of the joint axis rotations as

$${}^A\mathbf{R}_B = [\mathbf{u}, \mathbf{v}, \mathbf{w}] = \begin{bmatrix} \cos\alpha_z \cos\beta_z & -\sin\beta_x & \sin\alpha_y \cos\beta_y \\ \sin\alpha_z \cos\beta_z & \cos\alpha_x \cos\beta_x & -\sin\beta_y \\ -\sin\beta_z & \sin\alpha_x \cos\beta_x & \cos\alpha_y \cos\beta_y \end{bmatrix}, \tag{10}$$

where β_x, β_y, and β_z are the rotation angle of the second joint of each leg. If vector $\mathbf{s}$ is known, it means that the directions of the projections of vectors $\mathbf{u}$, $\mathbf{v}$, and $\mathbf{w}$ are known as well. In addition, the ratios between the projection components and the signs of these projection components will be understood. With this logic, the rotation matrix can be re-written as

$${}^A\mathbf{R}_B = [\mathbf{u}, \mathbf{v}, \mathbf{w}] = \begin{bmatrix} \cos\alpha'_z\sqrt{1-c^2} & -a & \sin\alpha'_y\sqrt{1-b^2} \\ \sin\alpha'_z\sqrt{1-c^2} & \cos\alpha'_x\sqrt{1-a^2} & -b \\ -c & \sin\alpha'_x\sqrt{1-a^2} & \cos\alpha'_y\sqrt{1-b^2} \end{bmatrix}, \tag{11}$$

where

$$-1 \leq a, b, c \leq 1.$$

The dummy variables a, b, and c represent the direction ratios of the second angle of rotation of each leg. The meaning of a, b, and c is better explained with the help of Fig. 5, where a represents the x component of the vector $\mathbf{d}^{\mathrm{u}}_{1,x}$ while the length of $\boldsymbol{k}_{Ax}$ is equal to $\sqrt{1-a^2}$ representing the projection of $\mathbf{d}^{\mathrm{u}}_{1,x}$ in the $y'z'$ plane. The meaning of b and c is explained in similar way.

Now, we divide the unit vectors $\mathbf{u}$, $\mathbf{v}$, and $\mathbf{w}$ in Eq. (11) by $\sqrt{1-c^2}$, $\sqrt{1-a^2}$, and$\sqrt{1-b^2}$, respectively. Note that this operation does not alter the direction ratios of vectors $\mathbf{u}$, $\mathbf{v}$, and $\mathbf{w}$. Accordingly, we will obtain the following three new vectors pointing at the same directions of $\mathbf{u}$, $\mathbf{v}$, and $\mathbf{w}$:

$$[\mathbf{u}', \mathbf{v}', \mathbf{w}'] = \begin{bmatrix} \cos\alpha'_z & -a' & \sin\alpha'_y \\ \sin\alpha'_z & \cos\alpha'_x & -b' \\ -c' & \sin\alpha'_x & \cos\alpha'_y \end{bmatrix},$$

with $a' = a/\sqrt{1-a^2}$, $b' = b/\sqrt{1-b^2}$, and $c' = c/\sqrt{1-c^2}$. The values of a', b', and c' can be evaluated by imposing mutual orthogonality to $\mathbf{u}'$, $\mathbf{v}'$, and $\mathbf{w}'$:

$$\mathbf{u}' \cdot \mathbf{v}' = 0, \mathbf{v}' \cdot \mathbf{w}' = 0, \mathbf{w}' \cdot \mathbf{u}' = 0,$$

which derives the following three equality equations:

$$\begin{cases} a' \sin\alpha'_y + b' \cos\alpha'_x - \cos\alpha'_y \sin\alpha'_x = 0 \\ b' \sin\alpha'_z + c' \cos\alpha'_y - \cos\alpha'_z \sin\alpha'_y = 0 \\ c' \sin\alpha'_x + a' \cos\alpha'_z - \cos\alpha'_x \sin\alpha'_z = 0 \end{cases}. \tag{12}$$

https://doi.org/10.1017/S0263574713001100 Published online by Cambridge University Press

Rearrange Eq. (12), then we have

$$\begin{bmatrix} \sin\alpha'_y & \cos\alpha'_x & 0 \\ 0 & \sin\alpha'_z & \cos\alpha'_y \\ \cos\alpha'_z & 0 & \sin\alpha'_x \end{bmatrix} \begin{bmatrix} a' \\ b' \\ c' \end{bmatrix} = \begin{bmatrix} \cos\alpha'_y \sin\alpha'_x \\ \cos\alpha'_z \sin\alpha'_y \\ \cos\alpha'_x \sin\alpha'_z \end{bmatrix}. \tag{13}$$

Equation (13) forms a linear system in a', b', and c' that can be solved as

$$\begin{cases} a' = \dfrac{\cos\alpha'_y \sin\alpha'_z - \cos\alpha'_x \cos\alpha'_z \sin\alpha'_y \sin\alpha'_x}{\Delta} \\ b' = \dfrac{\cos\alpha'_z \sin\alpha'_x - \sin\alpha'_y \cos\alpha'_x \sin\alpha'_z \cos\alpha'_y}{\Delta} \\ c' = \dfrac{\cos\alpha'_x \sin\alpha'_y - \cos\alpha'_z \cos\alpha'_y \sin\alpha'_x \sin\alpha'_z}{\Delta} \end{cases}, \tag{14}$$

where $\Delta = \cos\alpha'_z \cos\alpha'_y \cos\alpha'_x + \sin\alpha'_z \sin\alpha'_y \sin\alpha'_x$ is the determinant of the coefficients matrix of Eq. (13). Note that the condition for the existence of a unique solution (a', b', c') is that $\Delta \neq 0$. After a', b', and c' are found, the values of a, b, and c can be obtained by

$$a = a'\sqrt{1+(a')^2}, b = b'\sqrt{1+(b')^2}, \quad \text{and } c = c'\sqrt{1+(c')^2}.$$

So, it turns out that, when the projective angles, α_x, α_y, and α_z, are given, the rotation matrix ${}^A\mathbf{R}_B$ can be determined and is unique provided that $\Delta \neq 0$. So, for a given rotation matrix, there is a unique set of *projective angles* and *vice versa*. However, we should particularly notice that it does not imply that the solution for the inverse kinematics problem is unique. Each projective angle can correspond to two input angles, so there are eight possible combinations of the input angles based on a given set of the three projective angles. On the other hand, for some values of the projective angles, the determinant Δ is negative and in this case the determinant of the rotation matrix is also negative. This fact corresponds to a left-handed frame, which is unacceptable. Therefore, the projective angles must respect the condition $\Delta > 0$.

On the other hand, we should notice that the rotation matrix will be undetermined when $\Delta = 0$. At this situation, the mechanism meets its singular configurations where the projective vector(s) of the u-, v-, and/or w-axis disappear. For example, when $\alpha'_x = \pi/2$ and $\alpha'_y = \alpha'_z = 0$, the determinant $\Delta = 0$. In such a case, the w-axis is being perpendicular to the zx-plane so that the axis has no projective vector on the zx-plane.

6. Inverse Kinematics

6.1. Geometric reasoning

For the inverse kinematics problem, the orientation of the end-effector with respect to the fixed coordinate is given and the angular displacements of the R-joints, α_x, α_y, α_z, are to be found. Because the end-effector can only rotate about the center of the S-joint, the orientation of the end-effector is completely defined by its rotation matrix.

As shown in Fig. 5, we have learnt that the angular displacement, α_x, is fully dependent on the projective vector, $\mathbf{k}_{Ax}$. It implies that as long as $\mathbf{k}_{Ax}$ is determined, the angular displacement α_x can be obtained accordingly. Therefore, from the geometrical interpretation in Fig. 5, the angle between $\boldsymbol{k}_{Ax}$ and $\mathbf{y}'$ can be calculated by the equation below provided that $\mathbf{k}_{Ax}$ is a non-null projective vector of $\mathbf{d}^{\mathrm{u}}_{1,x}$ on Π_{Ax}:

$${}^v\theta_{yz} = \mathrm{atan2}(\mathbf{k}_{Ax,z}, \mathbf{k}_{Ax,y}). \tag{15}$$

Since $\mathbf{k}_{Ax} // \mathbf{d}^{\mathrm{u}}_{1,x} = \mathbf{v}$ and $\mathbf{k}_{Ax}$ is on plane $y'z'$, we can readily realize that $\mathbf{k}_{Ax} = [0, v_y, v_z]^{\mathrm{T}}$. Introducing $\mathbf{k}_{Ax} = [0, v_y, v_z]^{\mathrm{T}}$ into Eq. (15) and realizing there are two input angles corresponding

https://doi.org/10.1017/S0263574713001100 Published online by Cambridge University Press

to one projective angle, the input angle rotating about the x-axis, α_x, can be obtained as

$$\alpha_x = \text{atan2}(v_z, v_y) + k\pi, \quad \text{k} = 0 \text{ or } 1. \tag{16}$$

Similarly, by applying this analysis procedure to the other legs, two other input angles rotating about the y- and z-axis can be derived as

$$\alpha_y = \text{atan2}(w_x, w_z) + k\pi, \quad \text{k} = 0 \text{ or } 1, \tag{17}$$

and

$$\alpha_z = \text{atan2}(u_y, u_x) + k\pi, \text{k} = 0 \text{ or } 1. \tag{18}$$

Hence, when the rotation matrix ${}^A\mathbf{R}_B$ is given, there are two solutions in each of Eqs. (16)–(18). Therefore, for a given location of the end-effector, there are two corresponding input angles in each leg. It leads that there are eight possible solutions for the inverse kinematics problem for this mechanism.

In addition to the input angles, the joint displacements of the three P-joints in each leg are worth to be derived. According to Fig. 4, the loop equation of the leg mounted on the x-axis can be written as

$$\mathbf{d}_{1,x} + \mathbf{d}_{2,x} - \mathbf{d}_{3,x} = \mathbf{e} - \mathbf{a}_x. \tag{19}$$

Note that $\mathbf{a}_x$ is a given geometric parameter and $\mathbf{e}$ can be obtained when the rotation matrix ${}^A\mathbf{R}_B$ and an arbitrary point E are defined. Furthermore, due to the geometric constraint, the following equations hold simultaneously in any configuration:

$$\mathbf{d}_{1,x} = d_{1,x}\mathbf{v}, \tag{20}$$

$$\mathbf{d}_{2,x} = d_{2,x}\mathbf{w}, \tag{21}$$

$$\mathbf{d}_{3,x} = d_{3,x}\mathbf{u}, \tag{22}$$

where $d_{1,x}$, $d_{2,x}$, and $d_{3,x}$ are the representative lengths of vectors $\mathbf{d}_{1,x}$, $\mathbf{d}_{2,x}$, and $\mathbf{d}_{3,x}$, and the unit vectors $\mathbf{u}$, $\mathbf{v}$, and $\mathbf{w}$ have been given by the rotation matrix. Substituting Eqs. (20)–(22) into Eq. (19) and expressing Eq. (19) in three scalar equations concludes a system of three linear equations with three unknowns: d_1, d_2, and d_3. Accordingly, the representative lengths of the three P-joints can be solved.

6.2. Verification from the rotation matrix

The derivation of the inverse kinematics solution can be verified through the reasoning of the rotation matrix.

In analogy with Eqs. (9)–(11) in Section 5, we can evaluate the input angle vector $\mathbf{q}$ as

$$\mathbf{q} = \begin{bmatrix} \alpha_x \\ \alpha_y \\ \alpha_z \end{bmatrix} = \begin{bmatrix} \text{atan2}(v_z, v_y) + k_x\pi \\ \text{atan2}(w_x, w_z) + k_y\pi \\ \text{atan2}(u_y, u_x) + k_z\pi \end{bmatrix}, \quad k_x, k_y, k_z = 0, 1,$$

where k_x, k_y, and k_z indicates that for any value of sine function there are two values of cosine function. So the vector $\mathbf{q}$ has totally $2^3 = 8$ possible solutions. It therefore proves the result as derived in Section 6.1.

6.3. Numerical example

Here, we give a numerical example for the inverse kinematics problem. Suppose that $\mathbf{u} = [0.3015, 0.9045, -0.3015]^{\text{T}}$, $\mathbf{v} = [-0.8165, 0.4082, 0.4082]^{\text{T}}$, and $\mathbf{w} = [0.4924, 0.1231, 0.8616]^{\text{T}}$. Based on Eqs. (16)–(18), the inverse kinematic solutions are computed as in Table 1.

https://doi.org/10.1017/S0263574713001100 Published online by Cambridge University Press

Table I. Numerical example of inverse kinematic solutions (Unit: radians).

No. of solutions	α_x	α_y	α_z
1	0.7854	0.5191	1.2490
2	0.7854	0.5191	4.3906
3	0.7854	3.6607	1.2490
4	0.7854	3.6607	4.3906
5	3.9270	0.5191	1.2490
6	3.9270	0.5191	4.3906
7	3.9270	3.6607	1.2490
8	3.9270	3.6607	4.3906

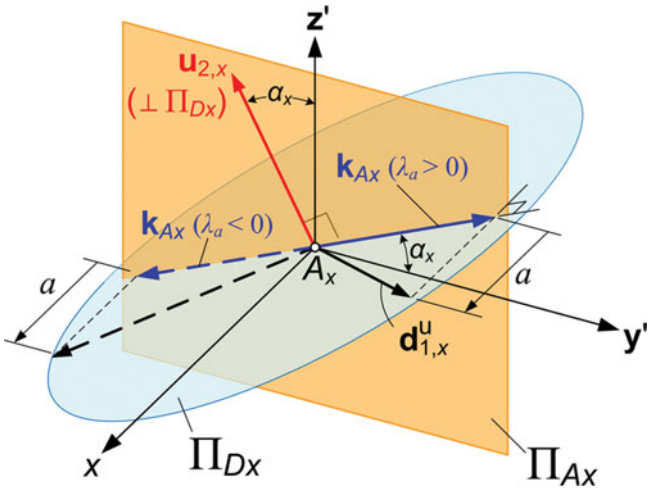

Fig. 6. (Colour online) Geometry for the direct kinematics problem.

7. Direct Kinematics

For the direct kinematics problem, the angular displacements of the R-joints are given and the location of the end-effector with respect to the fixed frame is to be found. Since the end-effector only possesses a 3-DOF rotational motion centered at the S-joint, the direct kinematics problem is reduced to the solving of the rotation matrix, ${}^{A}\mathbf{R}_{B}$.

7.1. Algebraic solution

The algebraic solution of the rotation matrix can be figured out based on the special geometrical relationship in the mechanism. Referring to Fig. 4, we know that based on the defined coordinate systems $\mathbf{d}_{1,x}$ is always parallel to the v-axis of the moving frame. Also, subject to the structural constraint of the U-joint, $\mathbf{d}_{1,x}$ is always perpendicular to $\mathbf{u}_{2,x}$. Considering the above two geometric constraints together, we can readily realize that all possible solutions of $\mathbf{d}_{1,x}$ will form a set of vectors lying on the plane that passes through A_x and is normal to $\mathbf{u}_{2,x}$. For illustrating this geometry, Fig. 6 is depicted. In this figure, plane Π_{Dx} is defined by its normal vector $\mathbf{u}_{2,x}$ and point A_x, and $\mathbf{d}^{\mathrm{u}}_{1,x}$, which is to be found, should locate on Π_{Dx}.

Therefore, when the actuated joint angle, α_x, is given, the vector $\mathbf{u}_{2,x}$ can be derived as

$$\mathbf{u}_{2,x} = [0, -\sin\alpha_x, \cos\alpha_x]^{\mathrm{T}}. \tag{23}$$

Furthermore, because $\mathbf{k}_{Ax}$ is a vector lying on Π_{Ax} and is perpendicular to $\mathbf{u}_{2,x}$, it can be expressed as

$$\mathbf{k}_{Ax} = [0, \lambda_a \cos\alpha_x, \lambda_a \sin\alpha_x]^{\mathrm{T}}, \tag{24}$$

https://doi.org/10.1017/S0263574713001100 Published online by Cambridge University Press

where $\|\lambda_a\|$ is the length of the vector. Since $\boldsymbol{k}_{Ax}$ is the projective vector of $\mathbf{d}^{\mathrm{u}}_{1,x}$ on plane Π_{Ax}, $\mathbf{d}^{\mathrm{u}}_{1,x}$ can be written as

$$\mathbf{d}^{\mathrm{u}}_{1,x} = [a, \lambda_a \cos\alpha_x, \lambda_a \sin\alpha_x]^{\mathrm{T}}. \tag{25}$$

Note that, as introduced in Eq. (11), variable a is related to the second angle of rotation of the leg. Besides, because $\mathbf{d}^{\mathrm{u}}_{1,x}$ is a unit vector, Eq. (25) should follow the identity equation of $\lambda_a^2 + a^2 = 1$.

Similarly, we can carry out the above analysis in the other two legs and obtain two equations in terms of $\mathbf{d}^{\mathrm{u}}_{1,y}$ and $\mathbf{d}^{\mathrm{u}}_{1,z}$ (which express the vectors of the first P-joint in the legs mounted on the y- and z-axis, respectively) and two associated identity equations. Therefore, having known the fact of $(\mathbf{u}, \mathbf{v}, \mathbf{w}) = (\mathbf{d}^{\mathrm{u}}_{1,z}, \mathbf{d}^{\mathrm{u}}_{1,x}, \mathbf{d}^{\mathrm{u}}_{1,y})$, we obtain

$$\mathbf{u} = [\lambda_c \cos\alpha_z, \lambda_c \sin\alpha_z, c]^{\mathrm{T}}, \tag{26}$$

$$\mathbf{v} = [a, \lambda_a \cos\alpha_x, \lambda_a \sin\alpha_x]^{\mathrm{T}}, \tag{27}$$

$$\mathbf{w} = [\lambda_b \sin\alpha_y, b, \lambda_b \cos\alpha_y]^{\mathrm{T}}, \tag{28}$$

subject to the three identity equations given below:

$$\lambda_a^2 + a^2 - 1 = 0, \tag{29}$$

$$\lambda_b^2 + b^2 - 1 = 0, \tag{30}$$

$$\lambda_c^2 + c^2 - 1 = 0. \tag{31}$$

Furthermore, since $\mathbf{u}$, $\mathbf{v}$, and $\mathbf{w}$ are three orthogonal vectors, the orthogonal conditions $\mathbf{u} \cdot \mathbf{v} = \mathbf{u} \cdot \mathbf{w} = \mathbf{v} \cdot \mathbf{w} = 0$ should be satisfied. Accordingly, based on Eqs. (26)–(28), the following three equations are obtained:

$$e_{11} a \lambda_c + e_{12} \lambda_a \lambda_c + e_{13} c \lambda_a = 0, \tag{32}$$

$$e_{21} \lambda_b \lambda_c + e_{22} b \lambda_c + e_{23} c \lambda_b = 0, \tag{33}$$

$$e_{31} a \lambda_b + e_{32} b \lambda_a + e_{33} \lambda_a \lambda_b = 0, \tag{34}$$

where e_{ij}, $i, j = 1$ to 3, are the coefficients given by α_x, α_y, and α_z. Equations (29) through (34) form a system of six second-degree polynomials in six unknowns: a, b, c, λ_a, λ_b, and λ_c. When the six unknowns are solved, the elements in the rotation matrix can be computed through Eqs. (26)–(28). Although the fundamental algebra theorem indicates that this system has at most $2^6 = 64$ solutions, a 3-homogeneous formulation[1] of the system shows that the maximum number of solutions of the homogeneous system can be reduced to 16. However, among these 16 solutions, eight ones will correspond to the trivial solutions:

$$\lambda_a = \lambda_b = \lambda_c = 0, a = \pm 1, b = \pm 1, c = \pm 1. \tag{35}$$

The above solutions correspond to the singular configurations of the manipulator that we will further discuss in Section 7.3. On the other hand, since half of the 16 solutions are conflicting the right-hand rule between $\mathbf{u}$, $\mathbf{v}$, and $\mathbf{w}$, we can conclude that the direct kinematics problem of this mechanism has at most eight possible solutions, four of which can be practically utilized.

7.2. Geometric reasoning

The algebraic solution of the direct kinematics for this mechanism can be realized by a geometrical reasoning. In Fig. 4, we showed that the v-axis of the moving coordinate must be parallel to $\mathbf{d}_{1,x}$. In Fig. 6, we learnt that $\mathbf{d}_{1,x}$ must lie on a plane whose normal vector $\mathbf{u}_{2,x}$ is defined by the input angle α_x. With these two geometric constraints, we can understand that the v-axis must lie on a plane, say

[1] Based on partitioning the six variables into three groups, (a, λ_a), (b, λ_b), and (c, λ_c), the 3-homogeneous Bezout number can be derived as 16.

https://doi.org/10.1017/S0263574713001100 Published online by Cambridge University Press

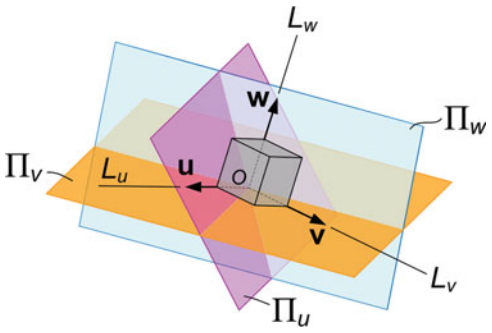

Fig. 7. (Colour online) Geometrical reasoning for the direct kinematics problem.

Π_v, which should pass through origin O and should be perpendicular to $\mathbf{u}_{2,x}$. In the same logic, the u- and w-axis must respectively lie on another two planes, say Π_w and Π_u, that are determined by origin O and by $\mathbf{u}_{2,y}$ and $\mathbf{u}_{2,z}$ (the two vectors defined by α_y and α_z), respectively. Accordingly, the direct kinematics problem of this mechanism is mapped onto a geometric problem, that is: Given three planes (Π_u, Π_v, and Π_w) with common intersection point O, identify three vectors, one from each plane (say $\mathbf{u}$ on Π_u, $\mathbf{v}$ on Π_v, and $\mathbf{w}$ on Π_w), such that

(1) each identified vector lies on a line that passes through point O;
(2) all identified vectors are perpendicular to each other; and
(3) all identified vectors obey the right-hand rule together (i.e., $\mathbf{u} \times \mathbf{v} = \mathbf{w}$).

Note that the above three conditions should be satisfied simultaneously. Apparently, this geometric problem is basically the searching of three, one from each plane, intersecting orthogonal lines. When the lines are found, each line will correspond two solutions for $\mathbf{u}$, $\mathbf{v}$, or $\mathbf{w}$ (i.e., two vectors pointing at opposite directions in the same line). Figure 7 demonstrates such a line-searching problem. As shown, in a general, non-singular geometry, we can find that there are at most one unique line on each plane, which are lines L_u on Π_u, L_v on Π_v, and L_w on Π_w. Line (L_u, L_v, L_w) forms one orthogonal set of lines, each corresponding to one solution space for accommodating the three vectors, $\mathbf{u}$, $\mathbf{v}$, and $\mathbf{w}$. Therefore, there will be $C_1^2 C_1^2 C_1^2 = 8$ possible combinations for ($\mathbf{u}$, $\mathbf{v}$, $\mathbf{w}$). However, only four of these eight are feasible due to the right-hand rule between $\mathbf{u}$, $\mathbf{v}$, and $\mathbf{w}$. This geometric validation proves the algebra solution as we derived above.

7.3. Verification from the rotation matrix

The reasoning of the direct kinematics described in Section 7.1 leads to the rotation matrix representing the angular position of the end-effector to be determined when the input angles α_x, α_y, and α_z are known.

$$ {}^{A}\mathbf{R}_B = [\mathbf{u}, \mathbf{v}, \mathbf{w}] = \begin{bmatrix} \lambda_c \cos\alpha_z & -a & \lambda_b \sin\alpha_y \\ \lambda_c \sin\alpha_z & \lambda_a \cos\alpha_x & -b \\ -c & \lambda_a \sin\alpha_x & \lambda_b \cos\alpha_y \end{bmatrix} \tag{36} $$

The matrix in Eq. (36) may be compared to those described in Section 5, notably to Eq. (10) and (11), from which we notice

$$ \begin{aligned} &a = \sin\beta_x, \lambda_a = \cos\beta_x, \quad \text{for } \lambda_a > 0 \text{ and } \lambda_a = \sqrt{1-a^2}; \\ &b = \sin\beta_y, \lambda_b = \cos\beta_y, \quad \text{for } \lambda_b > 0 \text{ and } \lambda_b = \sqrt{1-b^2}; \\ &c = \sin\beta_z, \lambda_c = \cos\beta_z, \quad \text{for } \lambda_c > 0 \text{ and } \lambda_c = \sqrt{1-c^2}. \end{aligned} \tag{37} $$

In particular it was proved that the matrix in Eq. (11) brought a unique solution for a, b, and c. Now the matrix in Eq. (36) may be considered a generalization of Eq. (11) where λ_a, λ_b, and λ_c may have positive or negative sign giving a total of eight possible combinations of sign and so the unique solutions of Eq. (11) generate eight solutions for Eq. (36). Moreover, it is evident that eight further solutions correspond to Eq. (35) obtaining a total of 16 different solutions. However half of these solutions correspond to left-handed frame and so cannot be accepted.

https://doi.org/10.1017/S0263574713001100 Published online by Cambridge University Press

As a total we have eight acceptable solutions, four of which, regardless of the values of the input angles, are:

$$ {}^{A}\mathbf{R}_{B} = \mathbf{R}_1 = \begin{bmatrix} 0 & 1 & 0 \\ 0 & 0 & 1 \\ 1 & 0 & 0 \end{bmatrix}, \tag{38a} $$

$$ {}^{A}\mathbf{R}_{B} = \mathbf{R}_2 = \begin{bmatrix} 0 & -1 & 0 \\ 0 & 0 & -1 \\ 1 & 0 & 0 \end{bmatrix}, \tag{38b} $$

$$ {}^{A}\mathbf{R}_{B} = \mathbf{R}_3 = \begin{bmatrix} 0 & 1 & 0 \\ 0 & 0 & -1 \\ -1 & 0 & 0 \end{bmatrix}, \tag{38c} $$

$$ {}^{A}\mathbf{R}_{B} = \mathbf{R}_4 = \begin{bmatrix} 0 & -1 & 0 \\ 0 & 0 & 1 \\ -1 & 0 & 0 \end{bmatrix}, \tag{38d} $$

while the other four solutions ($\mathbf{R}i$, $i = 5$ to 8) depend on the input angles.

Once one rotation matrix ${}^{A}\mathbf{R}_{B} = \mathbf{R}_5$ associated to one set of input angles is found, the other three solutions ($\mathbf{R}_6$, $\mathbf{R}_7$, $\mathbf{R}_8$) are immediately found as

$$ {}^{A}\mathbf{R}_{B} = \mathbf{R}_5 = [\,\mathbf{u}_s \quad \mathbf{v}_s \quad \mathbf{w}_s\,], \tag{39a} $$

$$ \mathbf{R}_6 = [\,\mathbf{u}_s \quad -\mathbf{v}_s \quad -\mathbf{w}_s\,], \tag{39b} $$

$$ \mathbf{R}_7 = [\,-\mathbf{u}_s \quad \mathbf{v}_s \quad -\mathbf{w}_s\,], \tag{39c} $$

$$ \mathbf{R}_8 = [\,-\mathbf{u}_s \quad -\mathbf{v}_s \quad \mathbf{w}_s\,]. \tag{39d} $$

So, given one set of input angles, we have eight possible rotation matrices corresponding to eight angular positions of the end-effector. However, it is important to notice that the four solutions of Eq. (38) correspond to singular orientations of the end-effector. In fact, for these angular positions, any values of the input angles is possible because the first and third joint axes of each leg are aligned and the projective angles are no more defined in that the unit vectors **u**, **v**, and **w** are orthogonal to the plane onto which the vectors must be projected. The four feasible solutions (solutions 5–8 in Eq. (39)) correspond to the four sets of projective angles:

$$ S_5 = \begin{bmatrix} \alpha'_{1x} \\ \alpha'_{1y} \\ \alpha'_{1z} \end{bmatrix} = \begin{bmatrix} \alpha_x \\ \alpha_y \\ \alpha_z \end{bmatrix}, \tag{40a} $$

$$ S_6 = \begin{bmatrix} \alpha'_{2x} \\ \alpha'_{2y} \\ \alpha'_{2z} \end{bmatrix} = \begin{bmatrix} \alpha_x \\ \alpha_y + \pi \\ \alpha_z + \pi \end{bmatrix}, \tag{40b} $$

$$ S_7 = \begin{bmatrix} \alpha'_{3x} \\ \alpha'_{3y} \\ \alpha'_{3z} \end{bmatrix} = \begin{bmatrix} \alpha_x + \pi \\ \alpha_y \\ \alpha_z + \pi \end{bmatrix}, \tag{40c} $$

$$ S_8 = \begin{bmatrix} \alpha'_{4x} \\ \alpha'_{4y} \\ \alpha'_{4z} \end{bmatrix} = \begin{bmatrix} \alpha_x + \pi \\ \alpha_y + \pi \\ \alpha_z \end{bmatrix}. \tag{40d} $$

https://doi.org/10.1017/S0263574713001100 Published online by Cambridge University Press

8. Conclusions

A fully decoupled 3-DOF parallel orientation mechanism has been introduced in this paper. The proposed mechanism is non-overconstrained variant of Agile Eye, and it possesses a special decoupled relationship between the projective angles of the moving frames and the input angles of the actuators at any instant. For studying this mechanism, the geometry of the mechanism was analyzed, and its fully decoupled kinematics was proven. Such a decoupled kinematics was also verified from the derivation of rotation matrix by using the projective angles. In addition, the inverse and direct kinematics problems of the mechanism were studied. It was found that there are at most eight possible solutions for the inverse kinematics problem and at most eight possible solutions for the direct kinematics problems, four of which correspond to singular positions of the end-effector and the other four can be practically utilized. The geometric reasoning for the position kinematics was carried out for validating the algebraic solutions. As a result, the proposed mechanism suggests a new mechanism topology for the orientation devices that require reduced alignment demands when in manufacturing.

Acknowledgements

The authors are thankful for the valuable comments and suggestions from the anonymous reviewers.

References

1. C. M. Gosselin and E. Lavoie, "On the kinematic design of spherical three-degree-of-freedom parallel manipulators," *Int. J. Robot. Res.* **12**(4), 394–402 (1993).
2. C. M. Gosselin, J. Sefrioui and M. J. Richard, "On the direct kinematics of spherical three-degree-of-freedom parallel manipulators of general architecture," *ASME J. Mech. Des.* **116**(2), 594–598 (1994).
3. X. Kong and C. M. Gosselin, "A formula that produces a unique solution to the forward displacement analysis of a quadratic spherical parallel manipulator: The Agile Eye," *ASME J. Mech. Robot.* **2**(4), 044501 (2010).
4. X. Kong and C. M. Gosselin, "Type synthesis of three-degree-of-freedom spherical parallel manipulators," *Int. J. Robot. Res.* **23**(3), 237–245 (2004).
5. X. Kong and C. M. Gosselin, "Type synthesis of 3-DOF spherical parallel manipulators based on screw theory," *ASME J. Mech. Des.* **126**(1), 101–126 (2004).
6. Y. Fang and L.-W. Tsai, "Structure synthesis of a class of 3-DOF rotational parallel manipulators," *IEEE Trans. Robot. Autom.* **20**(1), 117–121 (2004).
7. M. Karouia and J. M. Hervé, "Asymmetrical 3-Dof spherical parallel mechanisms," *Eur. J. Mech. A* **24**(1), 47–57 (2005).
8. T. A. Hess-Coelho, "Topological synthesis of a parallel wrist mechanism," *ASME J. Mech. Des.* **128**(1), 230–235 (2006).
9. M. Karouia and J. M. Hervé, "A three-DOF tripod for generating spherical rotation," **In**: *Advances in Robot Kinematics* (J. Lenarčić and M. M. Stanišić, eds.) (Kluwer Academic, London, 2000) pp. 395–402.
10. R. Di Gregorio, "Kinematics of a new spherical parallel manipulator with three equal legs: The 3-URC wrist," *J. Robot. Syst.* **18**(5), 213–219 (2001).
11. R. Di Gregorio, "A new parallel wrist using only revolute pairs: The 3-RUU wrist," *Robotica* **19**(3), 305–309 (2001).
12. R. Di Gregorio, "A new family of spherical parallel manipulators," *Robotica* **20**(4), 353–358 (2002).
13. R. Di Gregorio, "Kinematics of the 3-UPU wrist," *Mech. Mach. Theor.* **38**(3), 253–263 (2003).
14. R. Di Gregorio, "The 3-RRS wrist: A new, simple and non-overconstrained spherical parallel manipulator," *ASME J. Mech. Des.* **126**(5), 850–855 (2004).
15. R. Di Gregorio, "Kinematics of the 3-RSR wrist," *IEEE Trans. Robot.* **20**(4), 750–753 (2004).
16. M. Karouia and J. M. Hervé, "Non-overconstrained 3-Dof spherical parallel manipulators of type: 3-RCC, 3-CCR, 3-CRC," *Robotica* **24**(1), 85–94 (2006).
17. G. Gogu, "Fully-Isotropic Three-Degree-of-Freedom Parallel Wrists," *Proceedings of IEEE International Conference on Robotics and Automation*, Roma, Italy (Apr. 10–14, 2007) pp. 895–900.
18. J. Enferadi and A. A. Tootoonchi, "A novel spherical parallel manipulator: Forward position problem, singularity analysis, and isotropy design," *Robotica* **27**(5), 663–676 (2009).
19. R. Baumann, W. Maeder, D. Glauser and R. Clavel, "The PantoScope: A Spherical Remote-Center-of-Motion Parallel Manipulator for Force Reflection," *Proceedings of IEEE International Conference on Robotics and Automation*, Albuquerque, New Mexico, USA (Apr. 20–25, 1997) pp. 718–723.
20. P. Vischer and R. Clavel, "Argos: A novel 3-DoF parallel wrist mechanism," *Int. J. Robot. Res.* **19**(1), 5–11 (2000).
21. C. Innocenti and V. Parenti-Castelli, "Echelon form solution of direct kinematics for the general fully-parallel spherical wrist," *Mech. Mach. Theor.* **28**(4), 553–561 (1993).
22. K. Wohlhart, "Displacement analysis of the general spherical Stewart platform," *Mech. Mach. Theor.* **29**(4), 581–589 (1994).

23. Z. Huang and Y. L. Yao, "A new closed-form kinematics of the generalized 3-DOF spherical parallel manipulator," *Robotica* **17**(5), 475–485 (1999).
24. G. Alici and B. Shirinzadeh, "Topology optimisation and singularity analysis of a 3-SPS parallel manipulator with a passive constraining spherical joint," *Mech. Mach. Theor.* **39**(2), 215–235 (2004).
25. M. Carricato and V. Parenti-Castelli, "A novel fully decoupled two-degrees-of-freedom parallel wrist," *Int. J. Robot. Res.* **23**(6), 661–667 (2004).
26. J. Gallardo, R. Rodríguez, M. Caudillo and J. M. Rico, "A family of spherical parallel manipulators with two legs," *Mech. Mach. Theor.* **43**(2), 201–216 (2008).
27. C.-H. Kuo and J. S. Dai, "Kinematics of a fully-decoupled remote center-of-motion parallel manipulator for minimally invasive surgery," *ASME J. Med. Devices* **6**(2), 021008 (2012).
28. C.-H. Kuo, "Projective-Angle-Based Rotation Matrix and Its Applications," *The Second IFToMM Asian Conference on Mechanism and Machine Science*, Tokyo, Japan (Nov. 7–10, 2012).
29. Y. Jin, I.-M. Chen and G. Yang, "Kinematic design of a family of 6-DOF partially decoupled parallel manipulators," *Mech. Mach. Theor.* **44**(5), 912–922 (2009).
30. G. Legnani, I. Fassi, H. Giberti, S. Cinquemani and D. Tosi, "A new isotropic and decoupled 6-DoF parallel manipulator," *Mech. Mac. Theor.* **58**, 64–81 (2012).

https://doi.org/10.1017/S0263574713001100 Published online by Cambridge University Press